Available online at www.sciencedirect.com
SCIENCE DIRECT
ELSEVIER
European Journal of Mechanics B/Fluids 23 (2004) 879–898
EUROPEAN JOURNAL OF MECHANICS B/FLUIDS

Two-layer hydraulic falls over an obstacle

Frédéric Dias *, Jean-Marc Vanden-Broeck [a,b]

[a] *Centre de mathématiques et de leurs applications, École normale supérieure de Cachan, 61, avenue du Président Wilson, 94235 Cachan cedex, France*

[b] *School of Mathematics, University of East Anglia, Norwich NR4 7TJ, UK*

Received 30 September 2003; received in revised form 25 March 2004; accepted 19 April 2004

Available online 28 May 2004

Abstract

Motions in a forced channel flow of two contiguous homogeneous fluids of different constant densities and different thicknesses are considered. The total depth is finite and the upper surface is constrained to be planar (rigid lid approximation). The forcing is due to a bottom obstruction. The existence of a critical thickness ratio, obtained when the square of the thickness ratio is equal to the density ratio, leads to major differences with the one-layer case. The present study concentrates on this critical case. Moreover it is restricted to hydraulic falls, which are steady flows over an obstacle providing a transition between a subcritical and a supercritical flow. A weakly nonlinear analysis is performed. At leading order the problem reduces to a forced modified Korteweg–de Vries equation which can be integrated exactly. The weakly nonlinear results are validated by comparison with a numerical integration of the full governing equations. The numerical method is based on boundary integral equation techniques. The differences with the one-layer case are the existence of a second family of subcritical hydraulic falls when the thickness ratio is below critical, and the existence of supercritical hydraulic falls described by four parameters instead of three for all thickness ratios.

Keywords: Hydraulic falls; Two-layer flows; Forced Korteweg–de Vries equation

1. Introduction

This paper deals with motion forced by obstacles in the flow of two contiguous homogeneous fluids of different constant densities and different thicknesses. The total depth is finite and the upper surface is constrained to be planar (rigid lid approximation). This is an excellent approximation in most oceanic situations (see for example [1]). A two-layer configuration allows a wider variety of possible flow situations than a one-layer configuration. A review of the one-layer case (one fluid layer bounded below by a rigid bottom and above by a free surface) can be found in [2]. The complexity of the two-layer configuration is due to the existence of a critical thickness ratio, obtained when the square of the thickness ratio is equal to the density ratio. As far as we know, no physical interpretation of this critical thickness ratio has been given yet although it has been known for over fifty years. The present paper is a continuation of the companion paper [3], in which only the non-critical case, i.e. the case when the ratio of layer depths is far from critical, was considered. This companion paper will be referred to as DVB below. A summary of the results obtained in DVB is shown in Fig. 1. A hydraulic fall solution is characterized by different uniform flows upstream and downstream of the forcing. Fig. 1(a) shows that for a given obstruction, a given density ratio, and a ratio of layer depths above critical, there are two important values of the Froude number F, a subcritical one F_{sub} and a supercritical one F_{super}, such that:

* Corresponding author.
E-mail address: frederic.dias@cmla.ens-cachan.fr (F. Dias).

0997-7546/$ – see front matter
doi:10.1016/j.euromechflu.2004.04.003

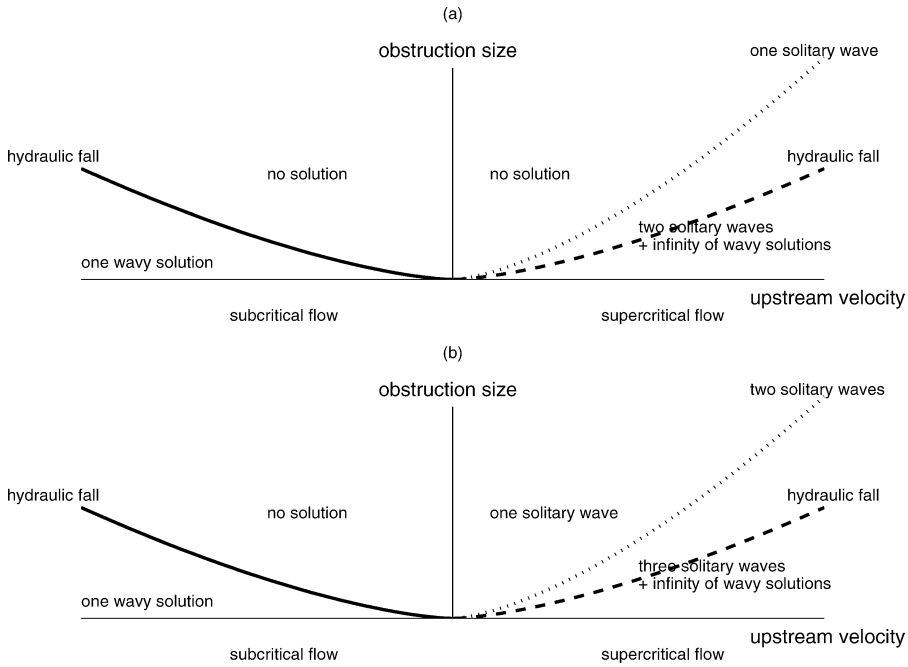

Fig. 1. Description of steady two-layer flows over an obstacle (from [3]). (a) Ratio of layer depths above critical. (b) Ratio of layer depths below critical. The positive (resp. negative) horizontal axis corresponds to supercritical (resp. subcritical) flows. The vertical axis is the obstacle size.

(i) when $F < F_{\text{sub}}$, there is a unique downstream periodic wave matched with the upstream (subcritical) uniform flow;
(ii) when $F = F_{\text{sub}}$, the period of the periodic wave extends to infinity and the solution becomes a hydraulic fall (conjugate flow solution) – the flow is subcritical upstream and supercritical downstream;
(iii) when $F > F_{\text{super}}$, there are two symmetric solitary waves sustained over the site of forcing, and at $F = F_{\text{super}}$ the two solitary waves merge into one;
(iv) when $F > F_{\text{super}}$, there is also a one-parameter family of solutions matching the upstream (supercritical) uniform flow with a periodic wave downstream;
(v) for a particular value of $F > F_{\text{super}}$, the downstream wave can be eliminated and the solution becomes a reversed hydraulic fall.

When the ratio of layer depths is below critical, Fig. 1(b) shows that the results are the same for subcritical flows. However, when the flow is supercritical, there is always an additional solitary wave solution, regardless of the size of the obstruction (this solution covers the whole 'supercritical' quarter plane).

In the present paper, we show that the consequences of the existence of a critical depth ratio are rather spectacular for solutions in the form of hydraulic falls. This is the reason why the emphasis of the paper is hydraulic falls. For the occurrence of hydraulic falls in nature, see for example [4].

An extensive literature review is available in [3]. Here we recall the main results. Sha and Vanden-Broeck [5] solved numerically an integrodifferential equation to compute two-layer flows past a semicircular obstruction, but their computations were restricted to symmetric solitary waves. Forbes [6] computed two-layer hydraulic falls with free-surface boundary conditions. In other words the top boundary is free. Belward and Forbes [7] computed two-layer flows over an arbitrary topography. Following [5,6], we choose the obstacle to be a semi-circular cylinder. As in [5], we only consider rigid tops. In other words the top boundary is a solid wall. Dias and Vanden-Broeck [8] computed two-layer fronts in the absence of obstacle and with a rigid top. Numerical computations of steady and unsteady internal waves can also be found in [9–11].

There are also results on model equations. Shen [12] derived forced Korteweg–de Vries equations for long nonlinear waves in two-layer flows with a free surface and compared his results with those of Forbes [6]. Capillary effects were included in [13,14]. Grimshaw, Chan and Chow [15] worked on a forced extended (or modified) Korteweg–de Vries equation. By extended, we mean a KdV equation with both a quadratic term and a cubic term in the nonlinearity. Hanazaki [16] compared time-dependent numerical results on model equations with results on the full equations. An interesting consequence of the vanishing of the quadratic term can be found in [17]. Johnson and Clarke worked on weakly nonlinear models for forced Rossby waves [18,19] and on supercritical leaps in two-layer hydraulics [20].

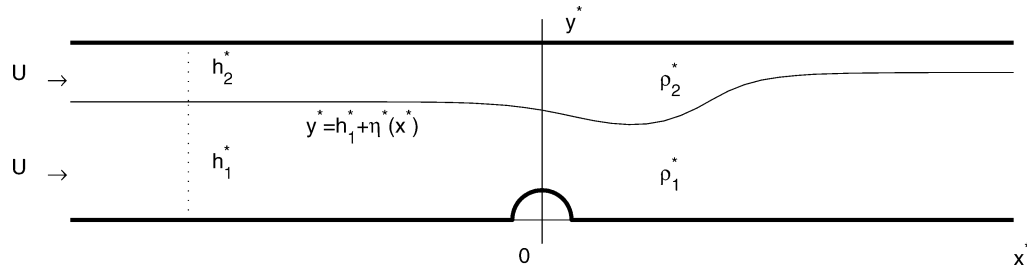

Fig. 2. Sketch of the flow. A uniform flow of velocity U in each layer approaches from left to right a semi-circular obstruction of radius r^*. The flow shown in the figure is a computed subcritical hydraulic fall, with parameters $\alpha = 0.2514$, $\beta = 0.5$, $\rho = 0.6$. The Froude number F, which is an unknown, is found to be to 0.304.

Various experimental results can be found in [21–26]. Pratt's experiments [22] deal with one-layer flows but they involve two obstacles. Pratt found some steady hydraulic falls with a regular train of waves between the obstacles, the flow being uniform and subcritical upstream of the first obstacle and uniform and supercritical downstream of the second obstacle. The focus of Melville and Helfrich's experiments [23] was the unsteady transcritical regime of two-layer flows over topography. They found a good agreement between their experiments and numerical solutions to a forced extended KdV equation for some range of parameters. Later, Grue et al. [9] found a very good agreement between the experiments and numerical solutions to the fully nonlinear equations for the full range of parameters. Arntsen [24,25] performed experiments on a submerged horizontal circular cylinder moving in a three-layer fluid. Measurements were made of the interfacial waves formed behind the cylinder towed horizontally at constant speeds, and of the drag and lift forces exerted on the cylinder. The closest experiments to the flows studied in the present paper are those of Lawrence [26]. Lawrence studied theoretically and experimentally steady two-layer flows over a fixed two-dimensional obstacle. He presented a classification scheme to predict the regime of flow given the obstacle size, the total depth of flow, and the density and flow rate of each layer. He found some differences between this classification scheme and that derived for flow over a towed obstacle by Baines [21]. These differences are due to the motion of upstream disturbances in towed obstacle flows. Lawrence observed various hydraulic falls and wavy solutions. He showed that internal hydraulic theory is not sufficient to explain the experimental results. Unfortunately, none of his experiments are near the critical case under study in the present paper.

The velocities of the uniform flows far upstream are assumed to be the same and are denoted by U. The thicknesses of the uniform flow far upstream are denoted by h_1^* (bottom layer) and h_2^* (upper layer). All along, quantities related to the upper layer of fluid will have the subscript 2, while those related to the bottom layer will be indexed with 1 (see Fig. 2). The upstream Froude number F is defined by

$$F = \frac{U}{\sqrt{gh_1^*}}, \tag{1}$$

where g is the acceleration due to gravity.

Section 2 provides the formulation of the problem. Our strategy is to find all solutions by weakly nonlinear analysis and to validate (or invalidate) them with numerical solutions of the full governing equations. In Section 3, a weakly nonlinear model is introduced. It is valid for subcritical as well as supercritical flows, close to the critical thickness ratio. In Section 4, the numerical scheme used to solve the full governing equations and boundary conditions is briefly described. Five regimes are considered and presented in Sections 5–9. Each regime is characterized by two properties: (i) subcritical or supercritical flow, and (ii) thickness ratio below, equal or above critical. The supercritical regime with critical thickness ratio is not described because hydraulic falls are not possible. Section 10 offers a discussion. The Appendix provides some exact properties of hydraulic falls.

2. Formulation

The steady irrotational flow of two contiguous incompressible inviscid fluids of different densities and different thicknesses past a submerged obstruction is considered (see Fig. 2). The x^*-axis is chosen to be along the bottom of the channel. The y^*-axis is chosen to go through the middle of the obstruction, which is assumed to be a semi-circle of radius r^*. The flow is assumed to be uniform far upstream, with the same velocity U in both layers. The densities are denoted by ρ_1^* (bottom layer) and ρ_2^* (top layer). The dimensionless circle radius α, the ratio of layer thicknesses β and the density ratio ρ are introduced:

$$\alpha = \frac{r^*}{h_1^*}, \quad \beta = \frac{h_2^*}{h_1^*}, \quad \rho = \frac{\rho_2^*}{\rho_1^*}. \tag{2}$$

The velocity potentials ϕ_i^* satisfy Laplace's equation in the interior of each layer:

$$\Delta\phi_i^* = 0, \quad i = 1, 2. \tag{3}$$

Along the interface described by $y^* = h_1^* + \eta^*(x^*)$ there are two kinematic conditions

$$\frac{\partial\phi_i^*}{\partial x^*}\frac{\mathrm{d}\eta^*}{\mathrm{d}x^*} - \frac{\partial\phi_i^*}{\partial y^*} = 0, \quad i = 1, 2. \tag{4}$$

Using Bernoulli's equation in each fluid and eliminating the pressure at the interface, one can write the dynamic condition in the form

$$\frac{1}{2}|\nabla\phi_1^*|^2 - \frac{1}{2}\rho|\nabla\phi_2^*|^2 + (1-\rho)g\eta^* = \frac{1}{2}(1-\rho)U^2. \tag{5}$$

The conditions of no flow normal to the upper and bottom walls may be written

$$\frac{\partial\phi_2^*}{\partial y^*} = 0 \quad \text{at } y^* = h_1^* + h_2^*, \quad \text{and} \quad \frac{\partial\phi_1^*}{\partial x^*}\frac{\mathrm{d}h^*}{\mathrm{d}x^*} = \frac{\partial\phi_1^*}{\partial y^*} \quad \text{at } y^* = h^*(x^*), \tag{6}$$

where

$$h^*(x^*) = \begin{cases} \left(r^{*2} - x^{*2}\right)^{1/2} & \left(|x^*| \leqslant r^*\right), \\ 0 & \left(|x^*| > r^*\right). \end{cases} \tag{7}$$

Let us briefly consider the linearization of the problem (3)–(6) in the absence of obstruction ($r^* = 0$). Given waves of the form

$$\phi_1^* = Ux^* + \varphi_1^*, \qquad \phi_2^* = Ux^* + \varphi_2^*,$$

the linearization results in the dispersion relation for infinitesimal waves of wavenumber k^* in a two-fluid configuration with a rigid lid:

$$k^*U^2\tanh k^*h_2^* + k^*U^2\rho\tanh k^*h_1^* = g(1-\rho)\tanh k^*h_1^*\tanh k^*h_2^*. \tag{8}$$

If the velocities of the uniform flows upstream were different in each layer (say U_1 and U_2), the dispersion relation would read

$$k^*U_1^2\tanh k^*h_2^* + k^*U_2^2\rho\tanh k^*h_1^* = g(1-\rho)\tanh k^*h_1^*\tanh k^*h_2^*.$$

In dimensionless form, the dispersion relation (8) becomes

$$kF^2(\tanh k\beta + \rho\tanh k) = (1-\rho)\tanh k\tanh k\beta, \tag{9}$$

where $k = k^*h_1^*$ is the dimensionless wavenumber. Real values for k can be found only if the Froude number F is smaller than F_{bif}, defined as

$$F_{\mathrm{bif}} = \sqrt{\frac{\beta(1-\rho)}{\beta+\rho}}. \tag{10}$$

The flow is then called subcritical. Otherwise it is supercritical.

In this paper, we look for stationary flows. The weakly nonlinear analysis as well as the numerical analysis deal with subcritical and supercritical flows. The focus is solutions in the form of hydraulic falls. For most solutions, the problem involves a set of three parameters, which can be chosen as (F, ρ, β) or (α, ρ, β). But in some cases, four parameters are needed to describe solutions. Some exact properties of hydraulic falls are summarized in the Appendix.

3. Weakly nonlinear analysis

One of the main difficulties in computing free-surface flows is to find the number of independent parameters. For that purpose, a weakly nonlinear analysis can be useful.

As shown in DVB, a classical perturbation expansion for long waves ($k \to 0$) applied to the problem (3)–(6) leads to the so-called forced Korteweg–de Vries (fKdV) equation. Since the present paper deals with stationary solutions, only the stationary fKdV equation is considered. Taking h_1^* as unit length and introducing

$$x = \frac{x^*}{h_1^*}, \quad \eta = \frac{\eta^*}{h_1^*}, \quad h = \frac{h^*}{h_1^*},$$

the fKdV equation takes the form

$$\frac{1}{6}b\eta_{xxx} + \frac{3}{2}a\eta\eta_x - (F - F_{\rm bif})\eta_x = -fh_x, \tag{11}$$

where

$$a = \frac{\beta^2 - \rho}{\beta(\beta+\rho)}F_{\rm bif}, \quad b = \beta\left(\frac{1+\beta\rho}{\beta+\rho}\right)F_{\rm bif}, \quad f = \frac{1}{2}\left(\frac{\beta}{\beta+\rho}\right)F_{\rm bif}. \tag{12}$$

The perturbation expansion depends on a small parameter ϵ. The scaling

$$x \to \sqrt{\epsilon}\frac{x}{\sqrt{b}}, \quad \eta \to \frac{1}{\epsilon}|a|\eta, \quad F - F_{\rm bif} = \epsilon\mu, \quad h \to \frac{1}{\epsilon^2}f|a|h \tag{13}$$

transforms (11) into

$$\frac{1}{6}\eta_{xxx} \pm \frac{3}{2}\eta\eta_x - \mu\eta_x = -h_x, \tag{14}$$

where the plus sign is chosen if $\beta > \sqrt{\rho}$ and the minus sign is chosen if $\beta < \sqrt{\rho}$. The parameter μ introduced in (13) is a bifurcation parameter. It measures the Froude number relative to the critical Froude number $F_{\rm bif}$. Integrating Eq. (14) once leads to

$$\eta_{xx} \pm \frac{9}{2}\eta^2 - 6\mu\eta = -3Q\delta(x), \tag{15}$$

under the condition that the flow is uniform far upstream, and that $h(x)$ can be approximated by the Dirac delta function:

$$h(x) = Q\delta(x).$$

This makes sense for obstructions whose height is comparable with the length of the obstruction base. It was shown in [2] that the scaling for Q is given by

$$Q \approx \alpha^{5/4}.$$

As explained in DVB, if $|\eta^*/h_1^*| \gg (\beta - \sqrt{\rho})$, that is near the critical ratio of layer depths $\beta = \sqrt{\rho}$, the fKdV equation is no longer valid. The coefficient a of the quadratic term $\eta\eta_x$ is small and the cubic term $\eta^2\eta_x$ must be computed. The previous long wave analysis was based on the scaling $\alpha = \epsilon^2$. The new scaling is $\alpha = \epsilon^3$ (see for example [13]). The modified KdV equation takes the form

$$\frac{1}{6}b\eta_{xxx} + \frac{3}{2}a\eta\eta_x - \frac{3}{4}c\eta^2\eta_x - (F - F_{\rm bif})\eta_x = -fh_x, \tag{16}$$

where

$$a = \frac{2(\beta - \sqrt{\rho})}{\sqrt{\rho}(1+\sqrt{\rho})}F_{\rm bif}, \quad b = (1 - \sqrt{\rho} + \rho)F_{\rm bif}, \quad c = \frac{4}{\sqrt{\rho}}F_{\rm bif}, \quad f = \frac{1}{2(1+\sqrt{\rho})}F_{\rm bif}.$$

The new scaling

$$x \to \epsilon\frac{x}{\sqrt{b}}, \quad \eta \to \frac{1}{\epsilon}\sqrt{c}\eta, \quad \frac{a}{\sqrt{c}} = \epsilon e, \quad F - F_{\rm bif} = \epsilon^2\mu, \quad h \to \frac{1}{\epsilon^3}f|a|h \tag{17}$$

transforms (16) into

$$\frac{1}{6}\eta_{xxx} + \frac{3}{2}e\eta\eta_x - \frac{3}{4}\eta^2\eta_x - \mu\eta_x = -h_x. \tag{18}$$

The parameter μ introduced in (17) is again a bifurcation parameter. It measures the Froude number relative to the critical Froude number $F_{\rm bif}$. The parameter e introduced in (17) measures how far one is from the critical ratio of layer depths $\beta = \sqrt{\rho}$. In the absence of forcing, the forced modified Korteweg–de Vries (fmKdV) equation (18) reduces to the modified Korteweg–de Vries equation (mKdV). Integrating (18) once leads to

$$\eta_{xx} + \frac{9}{2}e\eta^2 - \frac{3}{2}\eta^3 - 6\mu\eta = -3Q\delta(x), \tag{19}$$

under the condition that the flow is uniform far upstream, and that $h(x)$ can be approximated by the Dirac delta function:

$$h(x) = Q\delta(x).$$

One can show that the scaling for Q is given

$$Q \approx \alpha^{4/3}.$$

In order to study the solutions of the fmKdV equation (19), it is convenient to describe some properties of the mKdV equation ($Q = 0$). If $\mu > (9/16)e^2$, it has only one fixed point: $\eta = 0$. If $\mu < (9/16)e^2$, it has three fixed points:

$$\eta = 0 \quad (\mathrm{FP}_0), \quad \eta = \frac{3}{2}e - \frac{1}{2}\sqrt{9e^2 - 16\mu} \quad (\mathrm{FP}_1), \quad \eta = \frac{3}{2}e + \frac{1}{2}\sqrt{9e^2 - 16\mu} \quad (\mathrm{FP}_2). \tag{20}$$

If $e > 0$ and $\mu > 0$, the nontrivial fixed points are positive. If $e < 0$ and $\mu > 0$, the nontrivial fixed points are negative. If $\mu < 0$, one nontrivial fixed point is positive while the other one is negative. Interestingly enough, the number and the signs of fixed points of our model perfectly agree with those obtained from the full governing equations without any further assumption (see the Appendix).

Integrating the mKdV equation once leads to

$$\eta_x^2 = 6\mu\eta^2 - 3e\eta^3 + \frac{3}{4}\eta^4 + C. \tag{21}$$

Bounded solutions of (21) depend on μ and on e. As stated in the introduction, we will consider five cases. Indeed, we will consider the following cases: (i) subcritical flow ($\mu < 0$) or supercritical flow ($\mu > 0$), and (ii) thickness ratio below ($e < 0$), equal ($e = 0$) and above ($e > 0$) critical. The case of a supercritical flow with critical thickness ratio ($\mu > 0$ and $e = 0$) is not considered because there is only the trivial fixed point FP_0. For each case, the strategy will be the same: after studying the unforced case, we will study the forced case. The emphasis will be hydraulic falls. Solutions found through the weakly nonlinear analysis will be confirmed by means of a numerical integration of the full system of governing equations. This is why we provide in the next section the main steps of the numerical procedure.

4. Numerical scheme

Our numerical procedure follows closely the works of Sha and Vanden-Broeck [5] and of Dias and Vanden-Broeck [3]. Sha and Vanden-Broeck restricted their attention to solutions which are symmetric with respect to the y-axis. Here we follow [3] and relax this restriction in order to be able to compute hydraulic falls.

The problem is non-dimensionalised by using the velocity U as the reference velocity and the depth h_1^* as the reference length. The interface is described parametrically by $x = X(s)$ and $y = 1 + \eta = Y(s)$ where s is the arclength. Therefore we require

$$\big[X'(s)\big]^2 + \big[Y'(s)\big]^2 = 1, \tag{22}$$

where primes denote derivatives with respect to s. We choose $s = 0$ at the point $x = 0$ on the interface (i.e. $X(0) = 0$). Using the dimensionless variables, we rewrite (5) as

$$\frac{1}{2}\big[\phi_1'(s)\big]^2 - \frac{1}{2}\rho\big[\phi_2'(s)\big]^2 + \frac{1-\rho}{F^2}\big(Y(s) - 1\big) = \frac{1}{2}(1-\rho). \tag{23}$$

The bottom wall can be mapped into a straight line by using the Joukowski transformation. Following [5] and [3], we derive the integral equations

$$\begin{aligned} -\pi\big[\phi_2'(s)X'(s) - 1\big] = {} & \int_{-\infty}^{\infty} \frac{[\phi_2'(\sigma) - X'(\sigma)][Y(\sigma) - Y(s)] + [X(\sigma) - X(s)]Y'(\sigma)}{[X(\sigma) - X(s)]^2 + [Y(\sigma) - Y(s)]^2}\,\mathrm{d}\sigma \\ & + \int_{-\infty}^{\infty} \frac{[\phi_2'(\sigma) - X'(\sigma)][Y(\sigma) + Y(s) - 2\beta - 2] + [X(\sigma) - X(s)]Y'(\sigma)}{[X(\sigma) - X(s)]^2 + [2\beta + 2 - Y(\sigma) - Y(s)]^2}\,\mathrm{d}\sigma \end{aligned} \tag{24}$$

and

$$\begin{aligned} \pi\left[\frac{\phi_1'(s)f'(s)}{f'(s)^2 + g'(s)^2} - 2\right] = {} & \int_{-\infty}^{\infty} \frac{[\phi_1'(\sigma) - 2f'(\sigma)][g(\sigma) - g(s)] + 2[f(\sigma) - f(s)]g'(\sigma)}{[f(\sigma) - f(s)]^2 + [g(\sigma) - g(s)]^2}\,\mathrm{d}\sigma \\ & + \int_{-\infty}^{\infty} \frac{[\phi_1'(\sigma) - 2f'(\sigma)][g(\sigma) + g(s)] + 2[f(\sigma) - f(s)]g'(\sigma)}{[f(\sigma) - f(s)]^2 + [g(\sigma) + g(s)]^2}\,\mathrm{d}\sigma, \end{aligned} \tag{25}$$

where

$$f = \left(\frac{X}{2}\right)\frac{X^2+Y^2+\alpha^2}{X^2+Y^2}, \qquad g = \left(\frac{Y}{2}\right)\frac{X^2+Y^2-\alpha^2}{X^2+Y^2}. \tag{26}$$

We note that Eqs. (24) and (25) differ from Eqs. (5) and (8) in [5] because we did not assume symmetry with respect to the y-axis.

This concludes the formulation of the problem. For given values of β, ρ and α, we specify one of the two parameters $Y(0)$ or F and seek ϕ_1', ϕ_2', $X(s)$ and $Y(s)$ so that (23), (24) and (25) are satisfied.

These equations are discretised by following the procedures outlined in [5] and [3] and the resulting algebraic equations are solved by Newton iterations. The integrals from $-\infty$ to ∞ in (24) and (25) are replaced by integrals from $-A$ to B, where A and B are large. We improved the accuracy by approximating analytically the contributions to the integrals from $-\infty$ to $-A$ and from B to ∞. As $\sigma \to -\infty$, $\phi_1'(\sigma) \to 1$, $\phi_2'(\sigma) \to 1$, $X'(\sigma) \to 1$, $Y'(\sigma) \to 0$, $f'(\sigma) \to 1/2$ and $g'(\sigma) \to 0$. Therefore the numerators of the integrands in (24) and (25) tend to zero as $\sigma \to -\infty$ and we can neglect the contributions from $-\infty$ to $-A$ to the integrals. On the other hand, as $\sigma \to \infty$ the numerators of the integrands in (24) and (25) do not tend to zero. We evaluate the contribution from B to ∞ by replacing $\phi_1'(\sigma)$, $\phi_2'(\sigma)$, $Y(\sigma)$, $f(\sigma)$ and $g(\sigma)$ by their values at the last mesh point B and approximating $f'(\sigma)$ by $1/2$ and $g'(\sigma)$ by 0. The integrals from B to ∞ are then calculated analytically. We note that the approximations of the integrals are consistent in the sense that they become exact in the limit $A \to \infty$ and $B \to \infty$. In general the number of independent parameters for hydraulic falls is three. These three parameters are for example (F, ρ, β) or (α, ρ, β). But in some cases, four parameters are needed to describe hydraulic falls.

5. Subcritical flow upstream and $\beta > \sqrt{\rho}$

In this section and in the next four, we describe hydraulic falls for subcritical/supercritical flows and thickness ratios below/above critical. For a density ratio close to unity (fresh water on top of salt water for example), the critical thickness ratio is also close to unity. Therefore, when a less mathematical language is used below, the case of a thickness ratio above critical will be described as 'thick upper layer,' while the case of a thickness ratio below critical will be described as 'thin upper layer.'

The case considered in this section corresponds to $\mu < 0$ and $e > 0$ (subcritical flow and 'thick upper layer'). The fixed point FP_0 is a centre, while the two other fixed points FP_1 and FP_2 are saddle points. The phase plane of the mKdV equation (21) (no forcing) is shown in Fig. 3. The non-trivial bounded solutions are either periodic waves going around the centre FP_0, or a solitary wave going to the negative saddle point FP_1 at infinity. On the solitary wave solution, $\eta_x(\mathrm{FP}_1) = 0$. Therefore the constant C in (21) must be equal to

$$C_1 = -6\mu\eta_{\mathrm{FP}_1}^2 + 3e\eta_{\mathrm{FP}_1}^3 - \frac{3}{4}\eta_{\mathrm{FP}_1}^4 = -27\mu e^2 + 12\mu^2 + \frac{81}{8}e^4 + 6\mu e\sqrt{9e^2-16\mu} - \frac{27}{8}e^3\sqrt{9e^2-16\mu}.$$

Its asymptotic behavior as $\mu \to 0$ is

$$C_1 \approx \frac{32|\mu|^3}{9e^2}.$$

The phase plane shown in Fig. 3 is qualitatively similar to the KdV phase plane, except for the existence of the positive saddle point FP_2.

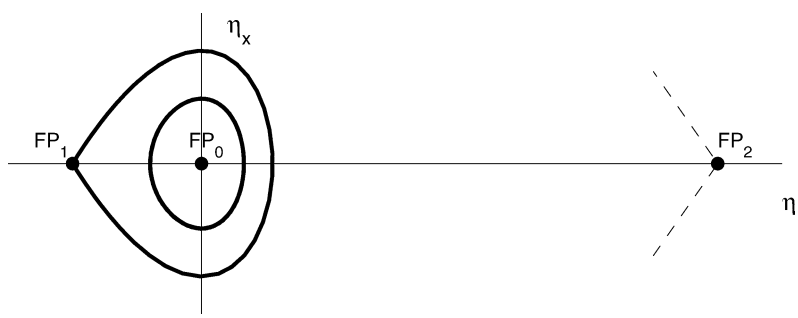

Fig. 3. Phase plane corresponding to Eq. (19) in the subcritical ($\mu < 0$) and unforced ($Q = 0$) case, with $e > 0$. The three fixed points are indicated. Some trajectories are shown (bounded, resp. unbounded, trajectories are plotted with solid, resp. dashed, lines).

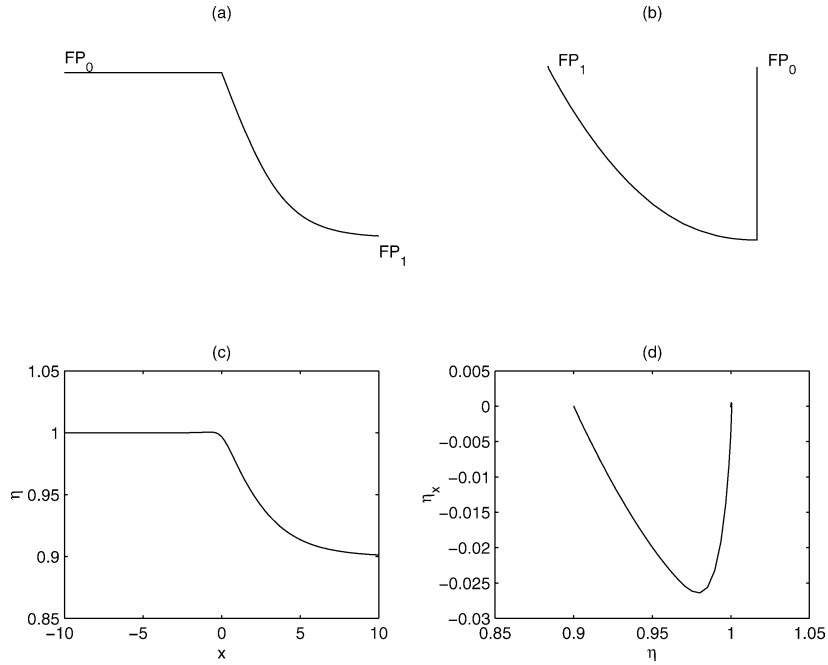

Fig. 4. Interface profile and phase plane of a subcritical hydraulic fall with $\beta > \sqrt{\rho}$. (a)–(b) Solution computed from the weakly nonlinear model. (c)–(d) Solution computed from the full equations. The thickness ratio is $\beta = 2$ and the density ratio is $\rho = 0.6$. Therefore $F_{\text{bif}} = 0.555$. The obstruction radius is $\alpha = 0.079$. The Froude number is found to be $F = 0.525$.

In the presence of forcing ($Q \neq 0$), we look for solutions which are continuous and bounded for $x \in \mathbb{R}$, and satisfy

$$\eta_{xx} + \frac{9}{2}e\eta^2 - \frac{3}{2}\eta^3 - 6\mu\eta = 0 \quad \text{for} \quad x \neq 0, \qquad \eta_x(0^+) - \eta_x(0^-) = -3Q. \tag{27}$$

The jump condition is obtained by integrating Eq. (19) from 0^- to 0^+.

Since the flow is assumed to be uniform upstream with $\eta = 0$, the solution at infinity upstream is necessarily $\eta = 0$ (see Fig. 2). Consequently the solution stays at FP_0 ($\eta = 0, \eta_x = 0$) for $x < 0$. At $x = 0^+$, the jump condition indicates that the slope of the interface must be $-3Q$. The only possibility for a bounded solution without oscillations in the far field downstream (hydraulic fall) is to jump from FP_0 on the homoclinic orbit. Since the value of η_x immediately after the jump is given by $-\sqrt{C_1}$, one has $Q(\mu; e) = \frac{1}{3}\sqrt{C_1}$. There is no restriction on the obstruction size, as μ decreases from 0 to $-\infty$. This solution corresponds to the curve "hydraulic fall" in the left quarter plane of Fig. 1(a). Both the interface profile and the corresponding phase plane are shown in Fig. 4. The solution was also computed using the numerical scheme described in Section 4. The qualitative agreement is good. At infinity downstream, the interface goes to the level given by the fixed point $\eta = \eta_{\text{FP1}}$.

6. Subcritical flow upstream and $\beta < \sqrt{\rho}$

The case considered in this section corresponds to $\mu < 0$ and $e < 0$ (subcritical flow and 'thin upper layer'). The fixed point FP_0 is a centre, while the two other fixed points are saddle points. The phase plane of the mKdV equation (21) (no forcing) is shown in Fig. 5. The non-trivial bounded solutions are either periodic waves going around the centre FP_0, or a solitary wave going to the positive saddle point FP_2 at infinity. On the solitary wave solution, $\eta_x(\text{FP}_2) = 0$. Therefore the constant C in (21) must be equal to

$$C_2 = -6\mu\eta_{\text{FP}_2}^2 + 3e\eta_{\text{FP}_2}^3 - \frac{3}{4}\eta_{\text{FP}_2}^4 = -27\mu e^2 + 12\mu^2 + \frac{81}{8}e^4 - 6\mu e\sqrt{9e^2 - 16\mu} + \frac{27}{8}e^3\sqrt{9e^2 - 16\mu}.$$

Its asymptotic behavior as $\mu \to 0$ is

$$C_2 \approx \frac{32|\mu|^3}{9e^2}.$$

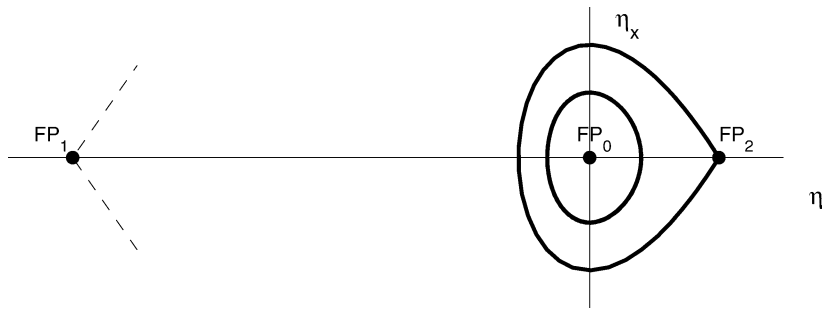

Fig. 5. Phase plane corresponding to Eq. (19) in the subcritical ($\mu < 0$) and unforced ($Q = 0$) case, with $e < 0$. The three fixed points are indicated. Some trajectories are shown (bounded, resp. unbounded, trajectories are plotted with solid, resp. dashed, lines).

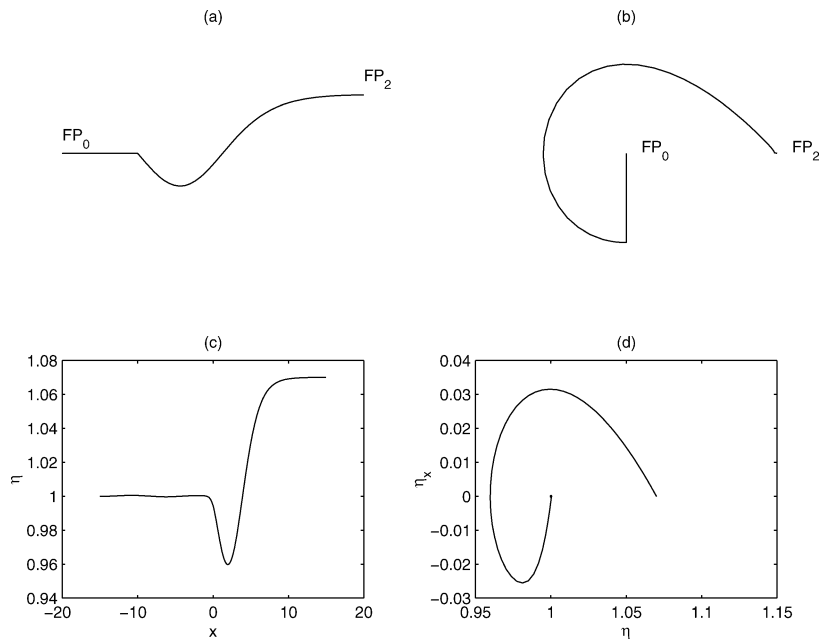

Fig. 6. Interface profile and phase plane of a subcritical hydraulic fall with $\beta < \sqrt{\rho}$. (a)–(b) Solution computed from the weakly nonlinear model. (c)–(d) Solution computed from the full equations. The thickness ratio is $\beta = 0.5$ and the density ratio is $\rho = 0.6$. Therefore $F_{\text{bif}} = 0.426$. The obstruction radius is $\alpha = 0.07$. The Froude number is found to be $F = 0.407$.

The phase plane shown in Fig. 5 is qualitatively similar to the KdV phase plane, except for the existence of the positive saddle point FP_1.

In the presence of forcing ($Q \neq 0$), we look for solutions which are continuous and bounded for $x \in \mathbb{R}$, and satisfy

$$\eta_{xx} + \frac{9}{2}e\eta^2 - \frac{3}{2}\eta^3 - 6\mu\eta = 0 \quad \text{for } x \neq 0, \qquad \eta_x(0^+) - \eta_x(0^-) = -3Q. \tag{28}$$

The jump condition is obtained by integrating Eq. (19) from 0^- to 0^+.

Since the flow is assumed to be uniform upstream with $\eta = 0$, the solution necessarily stays at FP_0 ($\eta = 0, \eta_x = 0$) for $x < 0$. At $x = 0^+$, the jump condition indicates that the slope of the interface must be $-3Q$. For hydraulic falls, we have two possibilities: either to jump from FP_0 on the homoclinic orbit, or to jump on the orbit going towards the negative fixed point FP_1.

For the solution which jumps on the homoclinic orbit, one has $Q(\mu; e) = \frac{1}{3}\sqrt{C_2}$ since the value of η_x immediately after the jump is given by $-\sqrt{C_2}$. This solution corresponds to the curve "hydraulic fall" in the left quarter plane of Fig. 1(b). Both the interface profile and the corresponding phase plane are shown in Fig. 6. The solution was also computed using the numerical scheme described in Section 4. The qualitative agreement is good. The profile shown in Fig. 2 is a solution of the same family.

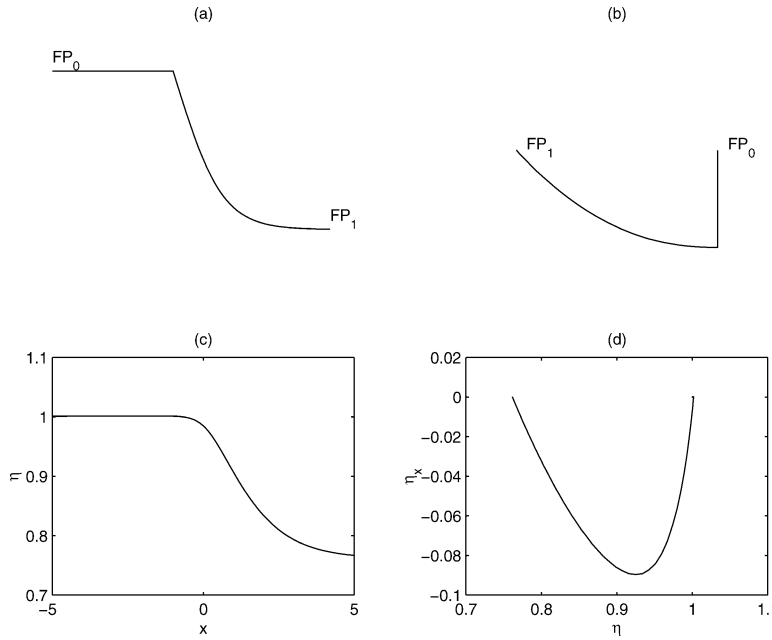

Fig. 7. Interface profile and phase plane of a subcritical hydraulic fall with $\beta < \sqrt{\rho}$. (a)–(b) Solution computed from the weakly nonlinear model. (c)–(d) Solution computed from the full equations. The thickness ratio is $\beta = 0.5$ and the density ratio is $\rho = 0.6$. Therefore $F_{\text{bif}} = 0.426$. The Froude number is equal to F_{bif} ($\mu = 0$). The obstruction radius is found to be $\alpha = 0.079$.

On the orbit going towards FP_1, $\eta_x(\text{FP}_1) = 0$. Therefore the constant C in (21) must be equal to

$$C_1 = -6\mu\eta_{\text{FP}_1}^2 + 3e\eta_{\text{FP}_1}^3 - \frac{3}{4}\eta_{\text{FP}_1}^4 = -27\mu e^2 + 12\mu^2 + \frac{81}{8}e^4 + 6\mu e\sqrt{9e^2 - 16\mu} - \frac{27}{8}e^3\sqrt{9e^2 - 16\mu}.$$

Since the value of η_x immediately after the jump is given by $-\sqrt{C_1}$, one has $Q(\mu; e) = \frac{1}{3}\sqrt{C_1}$. These solutions can be found if the obstruction is big enough ($Q > \frac{3}{2}e^2$). They persist even when $\mu = 0$, since $C_1(\mu = 0) = \frac{81}{4}e^4$. This type of hydraulic fall is new. It is due to the cubic nonlinearity. Both the interface profile and the corresponding phase plane are shown in Fig. 7. The solution was also computed using the numerical scheme described in Section 4. The qualitative agreement is good. This indicates that the modified KdV equation is a good model.

7. Subcritical flow upstream and $\beta = \sqrt{\rho}$

The case considered in this section corresponds to $\mu < 0$ and $e = 0$ (subcritical flow and upper and lower layers of 'equal' thicknesses). The fixed point FP_0 is a centre, while the two other fixed points FP_1 and FP_2 are saddle points. The phase plane of the mKdV equation (21) (no forcing) is shown in Fig. 8. The non-trivial bounded solutions are either periodic waves going around the centre FP_0, or fronts going from one saddle point to the other. On the front solution, $\eta_x(\text{FP}_1) = \eta_x(\text{FP}_2) = 0$. Therefore the constant C in (21) must be equal to $12|\mu|^2$.

When $C = 12|\mu|^2$,

$$\eta_x^2 = \frac{3}{4}\big(\eta - 2\sqrt{|\mu|}\big)^2\big(\eta + 2\sqrt{|\mu|}\big)^2. \tag{29}$$

The fronts connecting the two fixed points FP_1 and FP_2 at $\eta = \pm 2\sqrt{|\mu|}$ are given by

$$\eta(x) = \pm 2\sqrt{|\mu|}\tanh\big(\sqrt{3|\mu|}x\big). \tag{30}$$

In the presence of forcing ($Q \neq 0$), we look for solutions which are continuous and bounded for $x \in \mathbb{R}$, and satisfy

$$\eta_{xx} + \frac{9}{2}e\eta^2 - \frac{3}{2}\eta^3 - 6\mu\eta = 0 \quad \text{for } x \neq 0, \qquad \eta_x(0^+) - \eta_x(0^-) = -3Q. \tag{31}$$

Since the flow is assumed to be uniform upstream with $\eta = 0$, the solution necessarily stays at FP_0 ($\eta = 0, \eta_x = 0$) for $x < 0$. At $x = 0^+$, the jump condition indicates that the slope of the interface must be $-3Q$. For hydraulic falls, we have only one

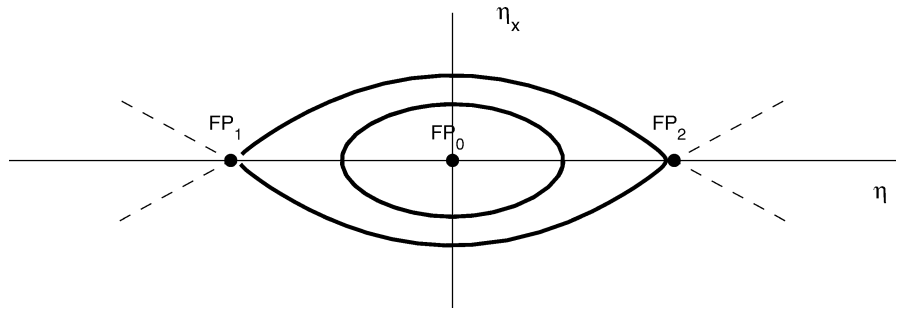

Fig. 8. Phase plane corresponding to Eq. (19) in the subcritical ($\mu < 0$) and unforced ($Q = 0$) case, with $e = 0$. The three fixed points are indicated. Some trajectories are shown (bounded, resp. unbounded, trajectories are plotted with solid, resp. dashed, lines).

possibility: to jump on the lower heteroclinic orbit. Since the value of η_x immediately after the jump is given by $-\sqrt{12}|\mu|$, one has $Q(\mu; e) = \frac{2}{\sqrt{3}}|\mu|$. There is no restriction on the obstruction size, as μ decreases from 0 to $-\infty$. Interface profiles and corresponding phase planes are not shown because they are qualitatively similar to those of Fig. 4.

8. Supercritical flow upstream and $\beta > \sqrt{\rho}$

The case considered in this section corresponds to $\mu > 0$ and $e > 0$ (supercritical flow and 'thick upper layer'). The fixed points FP_0 and FP_2 are saddle points, while the fixed point FP_1 is a center. As opposed to the subcritical case, the phase plane depends on μ. The critical values for μ are $\mu = \frac{1}{2}e^2$ and $\mu = \frac{9}{16}e^2$. The phase planes of the mKdV equation (21) (no forcing) are shown in Fig. 9. As explained in the Appendix, the value $\mu = \frac{1}{2}e^2$ corresponds to the value of the Froude number for fronts

$$F = F_{\text{front}} = \sqrt{\frac{(1+\beta)(1-\sqrt{\rho})}{1+\sqrt{\rho}}},$$

while the value $\mu = \frac{9}{16}e^2$ corresponds to the maximum value of the Froude number acceptable for hydraulic falls $F = F_{\max}$. It is quite remarkable that the mKdV equation reproduces (at least qualitatively) these two critical values of the Froude number obtained from the full governing equations, while the classical KdV equation reproduces none of these two values.

In Fig. 9(a), the non-trivial bounded solutions are either periodic waves going around the centre FP_1, or a solitary wave going to the origin FP_0 at infinity. On the solitary wave solution, $\eta_x(FP_0) = 0$. Therefore the constant C in (21) must be equal to 0. The phase plane shown in Fig. 9(a) is qualitatively similar to the KdV phase plane, except for the existence of the positive saddle point FP_2. Therefore, when $0 < \mu < \frac{1}{2}e^2$, all bounded solutions described in DVB also exist. There are in fact no other bounded solutions. In the presence of forcing ($Q \neq 0$), we look for solutions which are continuous and bounded for $x \in \mathbb{R}$, and satisfy

$$\eta_{xx} + \frac{9}{2}e\eta^2 - \frac{3}{2}\eta^3 - 6\mu\eta = 0 \quad \text{for } x \neq 0, \qquad \eta_x(0^+) - \eta_x(0^-) = -3Q. \tag{32}$$

The jump condition is obtained by integrating Eq. (19) from 0^- to 0^+.

Since the flow is assumed to be uniform upstream with $\eta = 0$, the solution for $x < 0$ necessarily follows the homoclinic orbit. At $x = 0$, the jump condition $\eta_x(0^+) - \eta_x(0^-) = -3Q$ must be satisfied. The only possibility for a bounded solution without oscillations in the far field downstream (hydraulic fall) is to jump on the fixed point FP_1. The value of η_x immediately before the jump is given by $\sqrt{6\mu\eta_{FP_1}^2 - 3e\eta_{FP_1}^3 + \frac{3}{4}\eta_{FP_1}^4}$. The solution for $x > 0$ simply is $\eta = \eta_{FP_1}$, $\eta_x = 0$. There is a one-to-one correspondance between μ and the obstruction size:

$$Q(\mu; e) = \frac{1}{3}\sqrt{6\mu\eta_{FP_1}^2 - 3e\eta_{FP_1}^3 + \frac{3}{4}\eta_{FP_1}^4}.$$

This solution corresponds to the curve labeled "hydraulic fall" in the right quarter plane of Fig. 1(a), except that it stops at $\mu = \frac{1}{2}e^2$. Both the interface profile and the corresponding phase plane are shown in Fig. 10. The solution was also computed using the numerical scheme described in Section 4. The qualitative agreement is good. At infinity downstream, the interface goes to the level given by the fixed point $\eta = \eta_{FP1}$.

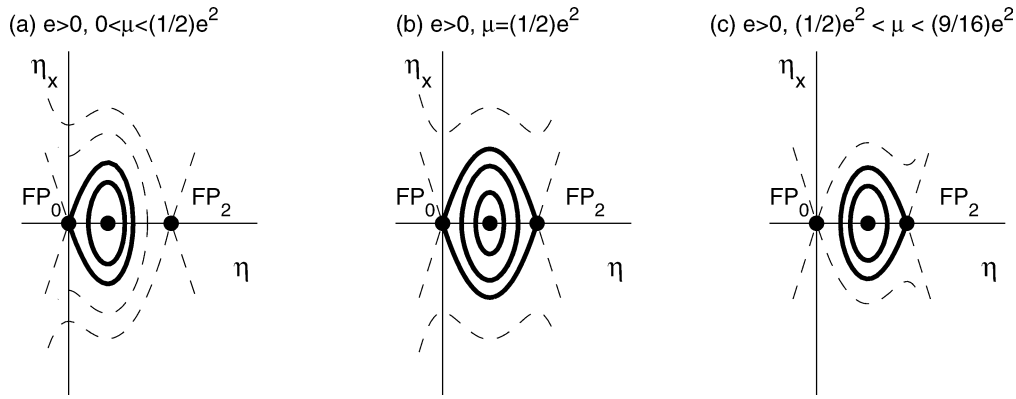

Fig. 9. Phase planes corresponding to Eq. (19) in the supercritical ($\mu > 0$) and unforced case ($Q = 0$), with $e > 0$. The phase plane for $\mu > (9/16)e^2$ is not shown: there is only one fixed point, the origin FP_0. In (b), the maximum value of η_x along the front is $\frac{1}{2}\sqrt{3}e^2$. The three fixed points are indicated. Some trajectories are shown (bounded, resp. unbounded, trajectories are plotted with solid, resp. dashed, lines).

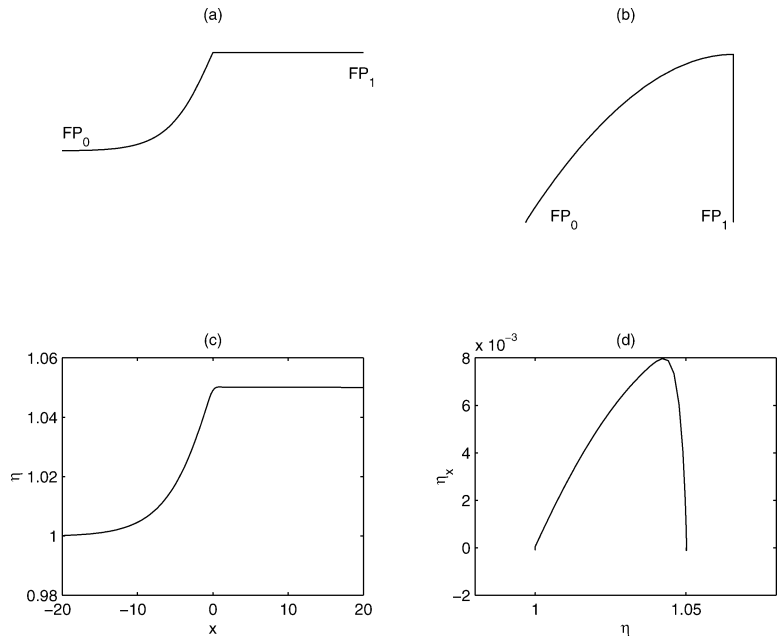

Fig. 10. Interface profile and phase plane of a supercritical hydraulic fall with $\beta > \sqrt{\rho}$ and $F_{\mathrm{bif}} < F < F_{\mathrm{front}}$. (a)–(b) Solution computed from the weakly nonlinear model. (c)–(d) Solution computed from the full equations. The thickness ratio is $\beta = 2$ and the density ratio is $\rho = 0.6$. Therefore $F_{\mathrm{bif}} = 0.555$ and $F_{\mathrm{front}} = 0.6173$. The obstruction radius is $\alpha = 0.046$. The Froude number is found to be $F = 0.568$.

The phase plane shown in Fig. 9(b) ($\mu = \frac{1}{2}e^2$) is different from the KdV phase plane. The non-trivial bounded solutions of (19) in the unforced case ($Q = 0$) are either periodic waves going around the centre FP_1, or fronts connecting the fixed points FP_0 and FP_2. The explicit expression of the front going from FP_0 to FP_2 is

$$\eta = e\left[1 + \tanh\left(\frac{1}{2}\sqrt{3}ex\right)\right]. \tag{33}$$

In the presence of forcing, the jump condition must be satisfied. Since the flow is assumed to be uniform upstream with $\eta = 0$, the solution for $x < 0$ necessarily follows the heteroclinic orbit. Again the only possibility for a bounded solution without oscillations in the far field downstream (hydraulic fall) is to jump at $x = 0$ from the heteroclinic orbit on the fixed point FP_1. The solution for $x > 0$ simply is $\eta = \eta_{\mathrm{FP}_1}$, $\eta_x = 0$.

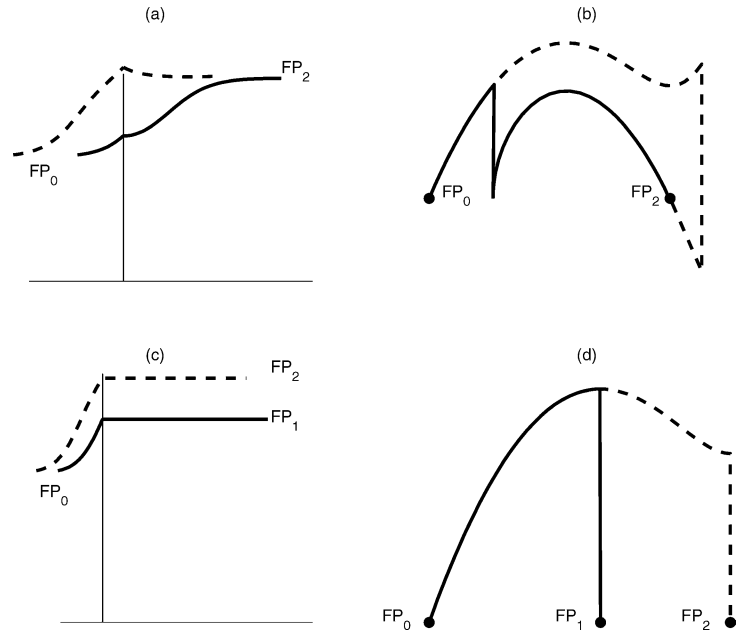

Fig. 11. Interface profiles and phase planes of various supercritical hydraulic falls obtained from the weakly nonlinear model with $\beta > \sqrt{\rho}$ and $F_{\text{front}} < F < F_{\max}$. (a)–(b) Solid line: solution connecting the unstable branch with the solitary wave of depression, dashed line: solution connecting both unstable branches. (c)–(d) Solutions connecting the unstable branch with the fixed point FP_1 (solid line) or the fixed point FP_2 (dashed line).

The phase plane shown in Fig. 9(c) ($\mu > \frac{1}{2}e^2$) is different from the KdV phase plane. The non-trivial bounded solutions are either periodic waves going around the centre FP_1, or a solitary wave going to the fixed point FP_2 at infinity. On the solitary wave solution, $\eta_x(\text{FP}_2) = 0$. Therefore the constant C in (21) must be equal to

$$C_2 = -6\mu\eta_{\text{FP}_2}^2 + 3e\eta_{\text{FP}_2}^3 - \frac{3}{4}\eta_{\text{FP}_2}^4 = -27\mu e^2 + 12\mu^2 + \frac{81}{8}e^4 - 6\mu e\sqrt{9e^2 - 16\mu} + \frac{27}{8}e^3\sqrt{9e^2 - 16\mu},$$

with

$$C_2\left(\mu = \frac{1}{2}e^2\right) = 0 \quad \text{and} \quad C_2\left(\mu = \frac{9}{16}e^2\right) = -\frac{81}{64}e^4.$$

In the presence of forcing, the jump condition must be satisfied. The solution for $x < 0$ necessarily follows the unbounded solution originating at the fixed point FP_0. At $x = 0$, the jump condition $\eta_x(0^+) - \eta_x(0^-) = -3Q$ must be satisfied. The situation here is different from all previous cases. Indeed, previous hydraulic falls were characterized by three independent parameters, for example the dimensionless obstacle size, the density ratio and the thickness ratio. In the weakly nonlinear analysis, these three parameters correspond to Q, ρ and β. The Froude number (or μ) is an unknown. This is still the case for the "classical" hydraulic falls where the solution jumps on the fixed point FP_1 (see the solid line in Fig. 11 (c) and (d)) or on the fixed point FP_2 (see the dashed line in Fig. 11 (c) and (d)). But a close look at the phase plane of Fig. 9(c) shows that one needs to specify the Froude number as well in order to obtain a hydraulic fall which goes to the fixed point FP_2, without jumping directly on it. Various possibilities are shown in Fig. 11. The jump can occur as soon as the elevation of the interface goes beyond the lowest point on the solitary wave of depression. Fig. 12 shows the jump magnitude (which is proportional to the obstruction size) as a function of the elevation where the jump occurs, for a particular set of parameters μ, ρ and β. In other words, four independent parameters are now needed to characterize a hydraulic fall. Moreover, for some sets of parameters (Q, μ, ρ, β), there can be as much as three distinct hydraulic falls (see Fig. 12). Note also that this new type of hydraulic falls requires a minimum obstruction size. Interface profiles and corresponding phase planes obtained numerically from the full equations are shown in Fig. 13 (classical hydraulic fall approching the fixed point FP_1 at infinity and corresponding to the curve labeled "hydraulic fall" in the right quarter plane of Fig. 1(a), except that it lies between the values F_{front} and $F_{\max}$ of the Froude number) and in Fig. 14 (hydraulic falls characterized by four independent parameters and approching the fixed point FP_2 at infinity).

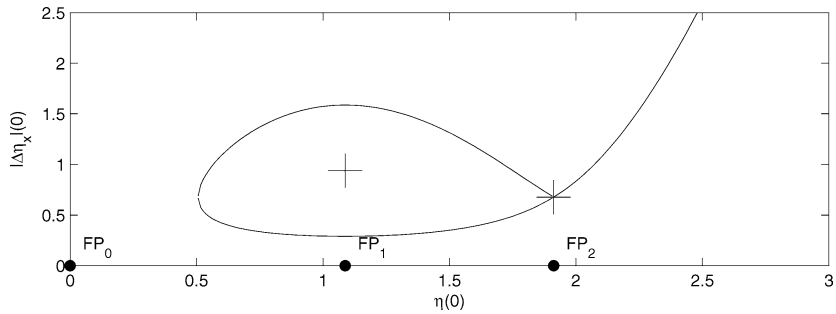

Fig. 12. In the supercritical case with $\beta > \sqrt{\rho}$ and $\frac{1}{2}e^2 < \mu < \frac{9}{16}e^2$, four parameters (Q, ρ, β, μ) are needed to describe hydraulic falls. The curve shows the jump magnitude at $x = 0$ (which is proportional to Q) versus the interface elevation where the jump occurs. The three other parameters ρ, β and μ are fixed. The "classical" hydraulic falls are indicated with + signs. The three fixed points are indicated.

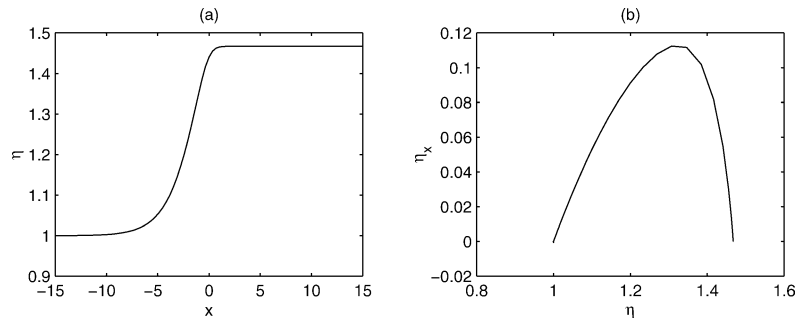

Fig. 13. Interface profile and phase plane of a supercritical hydraulic fall with $\beta > \sqrt{\rho}$ and $F_{\text{front}} < F < F_{\max}$. Solution computed from the full equations (this solution corresponds to the weakly nonlinear solution shown in Fig. 11 (c) and (d) with a solid line). The thickness ratio is $\beta = 2$ and the density ratio is $\rho = 0.6$. Therefore $F_{\text{bif}} = 0.555$, $F_{\text{front}} = 0.6173$, $F_{\max} = 0.6256$. The obstruction radius is $\alpha = 0.28$. The Froude number is found to be $F = 0.6250$.

9. Supercritical flow upstream and $\beta < \sqrt{\rho}$

The case considered in this section corresponds to $\mu > 0$ and $e < 0$ (supercritical flow and 'thin upper layer'). The fixed points FP_0 and FP_1 are saddle points, while the fixed point FP_2 is a center. As for the case $\beta > \sqrt{\rho}$, the phase plane depends on μ. Again, the critical values for μ are $\mu = \frac{1}{2}e^2$ and $\mu = \frac{9}{16}e^2$. The phase planes of the mKdV equation (21) (no forcing) are shown in Fig. 15.

The phase plane shown in Fig. 15(a) is qualitatively similar to the KdV phase plane, except for the existence of the negative saddle point FP_1. The non-trivial bounded solutions are either periodic waves going around the center FP_2, or a solitary wave going to the origin at infinity. On the solitary wave solution, $\eta_x(\text{FP}_0) = 0$. Therefore the constant C in (21) must be equal to 0.

In the presence of forcing, the jump condition must be satisfied. Since the flow is assumed to be uniform upstream with $\eta = 0$, the solution for $x < 0$ either follows the homoclinic orbit, or stays at the origin. The classical possibility for a bounded solution without oscillations in the far field downstream (hydraulic fall) is to jump from the homoclinic orbit on the fixed point FP_2. The solution for $x > 0$ simply is $\eta = \eta_{\text{FP}_2}$, $\eta_x = 0$. The presence of the fixed point FP_1 leads to a new possibility for hydraulic falls: it consists in leaving the origin along the homoclinic orbit (depression solitary wave) and jumping down on the unbounded orbit which goes back to the fixed point FP_1. A close look at the phase plane of Fig. 15(a) shows that in general one needs to specify the Froude number as well in order to obtain a hydraulic fall which goes to the fixed point FP_1. Various possibilities are shown in Fig. 16 (a) and (b). The jump can occur as long as the elevation of the interface immediately before the jump stays above the lowest point on the solitary wave of depression. Fig. 17 shows the jump magnitude (which is proportional to the obstruction size) as a function of the elevation where the jump occurs, for a particular set of parameters μ, ρ and β. In other words, four independent parameters are again needed to characterize a hydraulic fall. Moreover, for some sets of parameters (Q, μ, ρ, β), there can be as much as three distinct hydraulic falls (see Fig. 17). Again this type of hydraulic falls requires a minimum obstruction size.

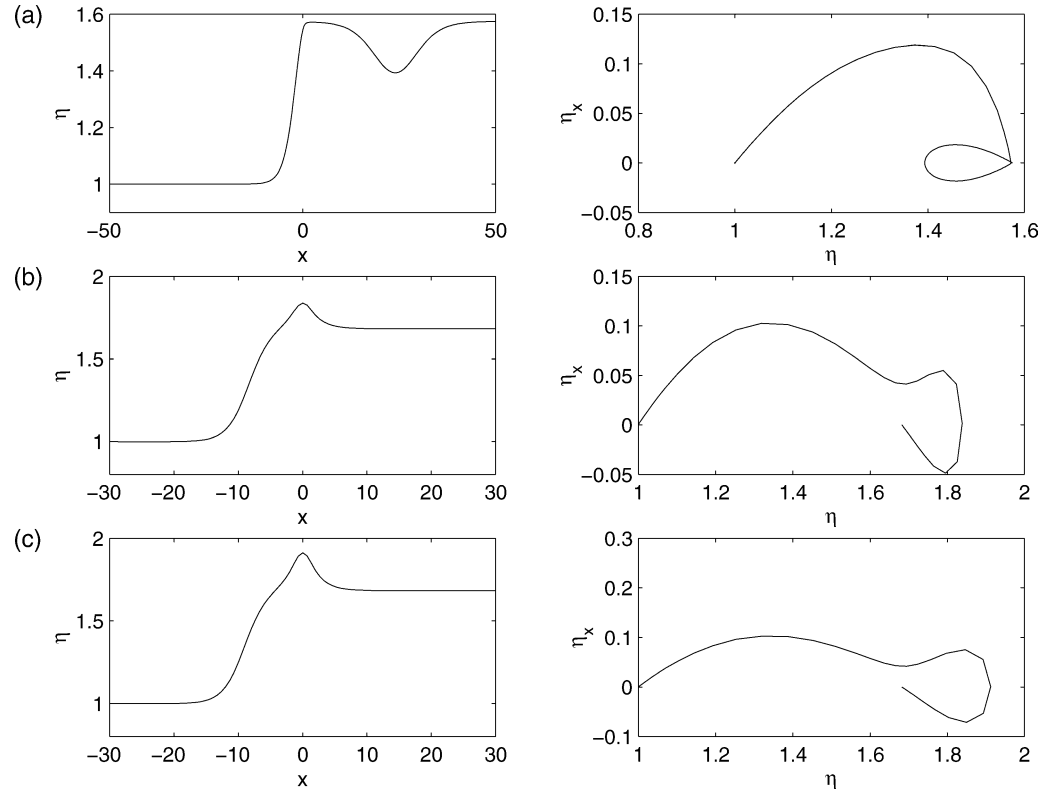

Fig. 14. Interface profiles and phase planes of various supercritical hydraulic falls with $\beta > \sqrt{\rho}$ and $F_{\text{front}} < F < F_{\max}$. Solutions computed from the full equations (these solutions correspond to the weakly nonlinear solutions shown in Fig. 11 (a) and (b)). The thickness ratio is $\beta = 2$ and the density ratio is $\rho = 0.6$. Therefore $F_{\text{bif}} = 0.555$, $F_{\text{front}} = 0.6173$, $F_{\max} = 0.6256$. The obstruction radius is, from top to bottom, $\alpha = 0.305, 0.65, 0.85$. The Froude number is found to be, from top to bottom, $F = 0.6247, 0.618, 0.618$.

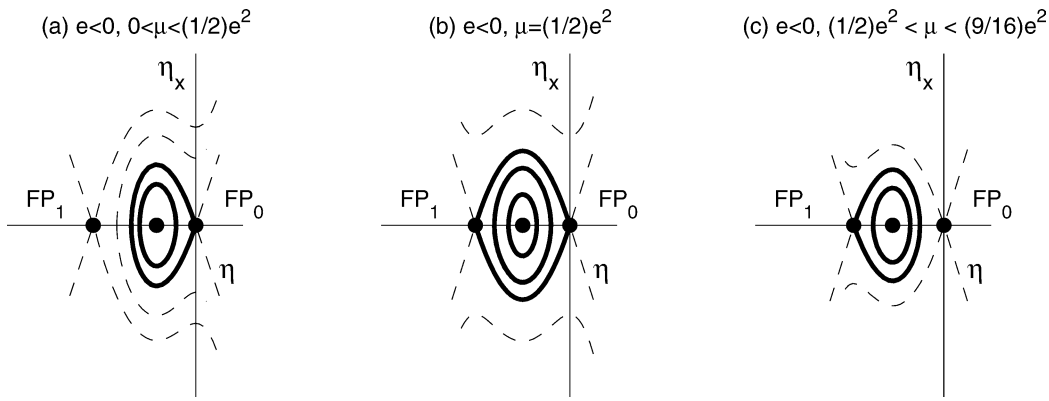

Fig. 15. Phase planes corresponding to Eq. (19) in the supercritical ($\mu > 0$) and unforced case ($Q = 0$), with $e < 0$. The phase plane for $\mu > (9/16)e^2$ is not shown: there is only one fixed point, the origin FP_0. In (b), the maximum value of η_x along the front is $\frac{1}{2}\sqrt{3}e^2$. The three fixed points are indicated. Some trajectories are shown (bounded, resp. unbounded, trajectories are plotted with solid, resp. dashed, lines).

Interface profiles and corresponding phase planes computed numerically from the full equations are shown in Fig. 18 (classical hydraulic fall approaching the fixed point FP_2 at infinity and corresponding to the curve labeled "hydraulic fall" in the right quarter plane of Fig. 1(b), except that it lies between the values F_{bif} and F_{front} of the Froude number) and in Fig. 19 (hydraulic falls characterized by four independent parameters and approaching the fixed point FP_1 at infinity).

Finally, a look at the phase planes shown in Fig. 15 (b) and (c) indicates that hydraulic falls are not possible for $F > F_{\text{front}}$.

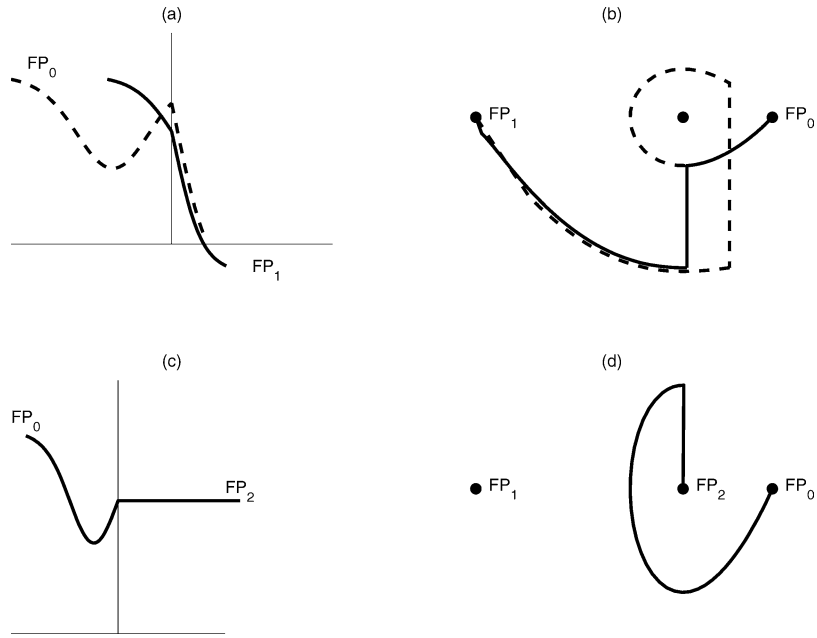

Fig. 16. Interface profiles and phase planes of various supercritical hydraulic falls obtained from the weakly nonlinear model with $\beta < \sqrt{\rho}$ and $F_{\text{bif}} < F < F_{\text{front}}$. (a)–(b) Solutions connecting the homoclinic orbit originating at the fixed point FP_0 with the unstable branch going to the fixed point FP_1. (c)–(d) Solution connecting the homoclinic orbit originating at the fixed point FP_0 with the fixed point FP_2.

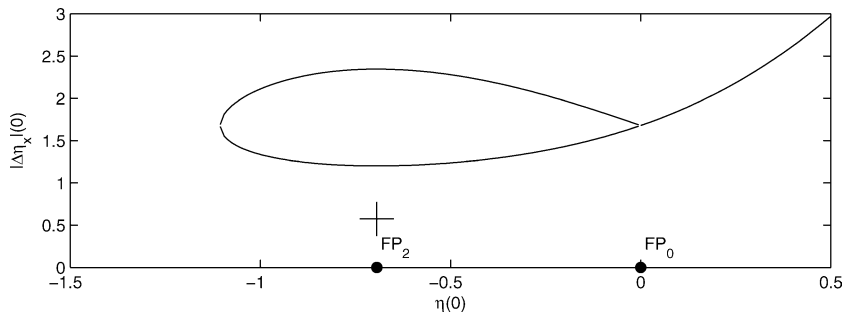

Fig. 17. In the supercritical case with $\beta < \sqrt{\rho}$ and $0 < \mu < \frac{1}{2}e^2$, four parameters (Q, ρ, β, μ) are needed to describe hydraulic falls. The curve shows the jump magnitude at $x = 0$ versus the interface elevation where the jump occurs. The "classical" hydraulic fall is indicated with a + sign. The two fixed points FP_2 and FP_0 are indicated.

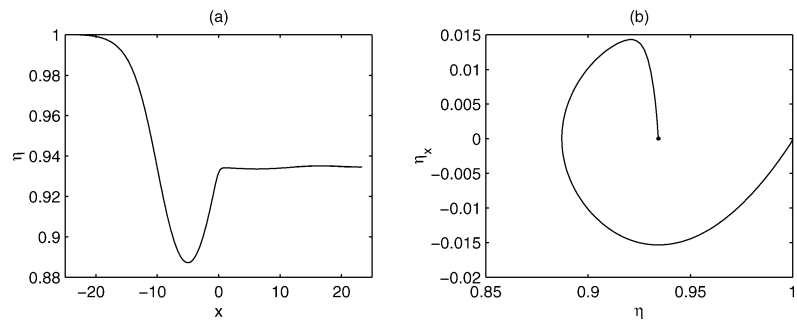

Fig. 18. Interface profile and phase plane of a supercritical hydraulic fall with $\beta < \sqrt{\rho}$ and $F_{\text{bif}} < F < F_{\text{front}}$. Solution computed from the full equations (this solution corresponds to the weakly nonlinear solution shown in Fig. 16 (c) and (d)). The thickness ratio is $\beta = 0.5046$ and the density ratio is $\rho = 0.6$. Therefore $F_{\text{bif}} = 0.4275$ and $F_{\text{front}} = 0.4372$. The obstruction radius is $\alpha = 0.0421$. The Froude number is found to be $F = 0.4365$.

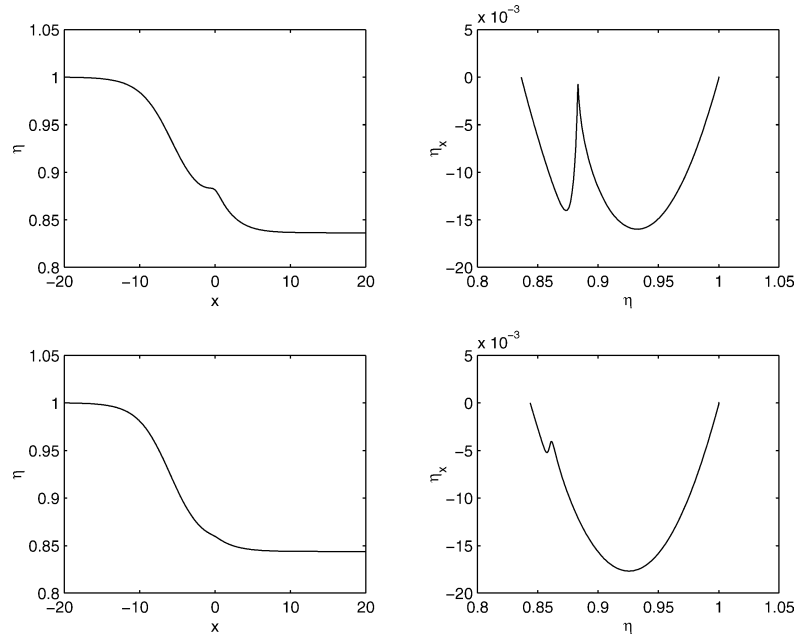

Fig. 19. Interface profiles and phase planes of various supercritical hydraulic falls with $\beta < \sqrt{\rho}$ and $F_{\rm bif} < F < F_{\rm front}$. Solutions computed from the full equations (these solutions correspond to the weakly nonlinear solutions shown in Fig. 16 (a) and (b)). The thickness ratio is $\beta = 0.5$ and the density ratio is $\rho = 0.6$. The Froude numbers are found to be $F = 0.4359$ (top) and $F = 0.4364$ (bottom).

10. Discussion

The analytical and numerical results found in DVB have been extended to the full range of Froude numbers and thickness ratios. We now have a full picture of hydraulic falls generated by an obstacle moving at a constant velocity at the bottom of a channel containing two superposed layers of fluids of constant densities. All hydraulic fall solutions of the asymptotic long wave equations have been identified. The equivalent solutions of the fully nonlinear equations have been computed. One interesting finding of the analytical studies is that the various families of hydraulic falls depend either on three or on four parameters. We have established that this is not an artifact of the long wave asymptotics by demonstrating that the same dependence on the number of parameters occurs in the fully nonlinear calculations.

Two important values of the Froude number have been known for a long time: the value $F_{\rm bif}$ corresponding to the transition subcritical/supercritical and the supercritical value $F_{\rm front}$ corresponding to fronts. Our present results show the importance of a third value, larger than the other two, $F_{\rm max}$. This is the maximum Froude number for hydraulic falls. Its importance in experiments has not been revealed yet, simply because the interval $[F_{\rm front}, F_{\rm max}]$ is usually rather small. For example, for $\rho = 0.6$ and $\beta = 0.5$, this interval is $[0.4365, 0.4377]$! For $\beta = 2$, it is $[0.6173, 0.6256]$. If one takes $\rho = 0.96$, a typical value for experiments, one finds $[0.1237, 0.1246]$ for $\beta = 0.5$ and $[0.1750, 0.1763]$ for $\beta = 2$. In fact even the whole range $[F_{\rm bif}; F_{\rm max}]$ is small since $F_{\rm bif} = 0.1170$ for $\beta = 0.5$ and $F_{\rm bif} = 0.1644$ for $\beta = 2$. Consider for example a channel with total depth equal to 30 cm. Then $\beta = 0.5$ is obtained with $h_1^* = 20$ cm ($h_2^* = 10$ cm) and $\beta = 2$ with $h_1^* = 10$ cm ($h_2^* = 20$ cm). The corresponding interesting interval range for the speed U is $[16.5; 17.6]$ cm/s for both thicknesses. In order to obtain a wider interval, one should take for example a thicker bottom layer $h_1^* = 27$ cm ($h_2^* = 3$ cm). The corresponding interval for U would be $[10.6; 18.3]$ cm/s. Recall that this is the region where the number of independent parameters for hydraulic falls is four instead of three. The consequence for experiments is as follows. Let us consider for example the simple experiment in which an obstacle moves at the bottom of a channel filled with two superposed fluids at rest. The known parameters are the density ratio ρ, the thickness ratio β and the obstruction size Q. Usually one expects only one value of the obstacle speed which provides an hydraulic fall. Our new results in the range $[F_{\rm bif}; F_{\rm max}]$ indicate that all values of the speed may provide an hydraulic fall! However, the speed range is rather small and only careful experiments may be able to explain what happens.

Fig. 20 provides a summary of the existence of hydraulic falls for two-layer flows. It is interesting to compare Fig. 20 with Fig. 1. All the curves labeled 'hydraulic fall' in Fig. 1 are also present in Fig. 20. But the supercritical curves stop either at $F = F_{\rm front}$ ($\beta < \sqrt{\rho}$) or at $F = F_{\rm max}$ ($\beta > \sqrt{\rho}$). Moreover there is a second branch of subcritical falls in the case $\beta < \sqrt{\rho}$. Finally, there is a region of supercritical hydraulic falls described by four parameters. As stated in the introduction, the focus of the present paper is hydraulic falls. As in DVB, there are other steady solutions: solitary waves, wavy solutions, generalized

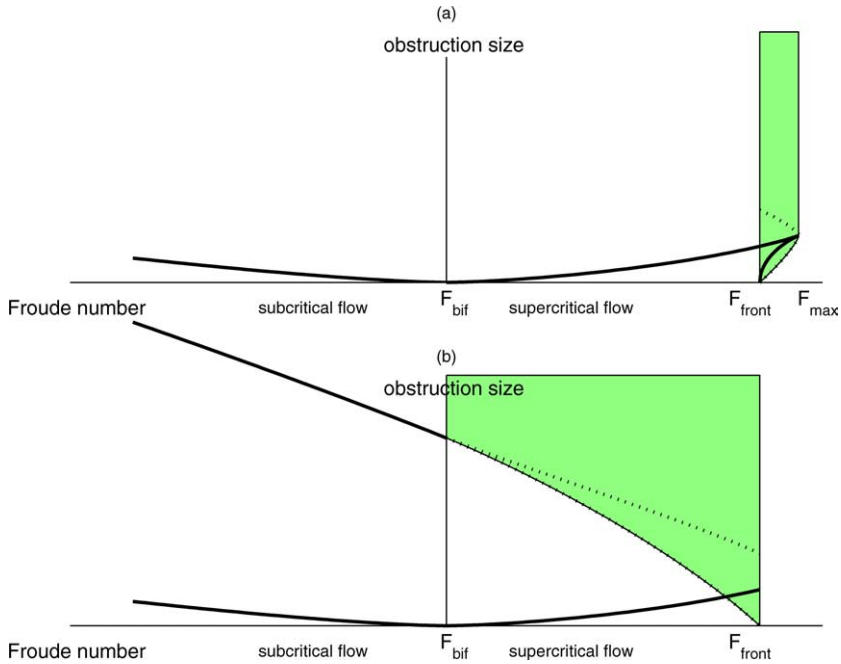

Fig. 20. Description of steady two-layer hydraulic falls over an obstacle. (a) Ratio of layer depths slightly above critical ($\beta > \sqrt{\rho}$). (b) Ratio of layer depths slightly below critical ($\beta < \sqrt{\rho}$). The positive (resp. negative) horizontal axis corresponds to supercritical (resp. subcritical) flows. The vertical axis is the obstacle size. The shaded regions represent hydraulic falls with four independant parameters. The dotted lines represent the lower and upper parts of the loops in Figs. 12 and 17.

hydraulic falls. Wavy solutions and generalized hydraulic falls approach a periodic solution downstream. In fact, the solutions shown in Fig. 6 and in Fig. 18 are generalized hydraulic falls. One can see small waves along the interface.

A final remark is that there is a shear layer downstream for hydraulic falls. In the absence of interfacial tension, instabilities of Kelvin–Helmholtz type may develop. Therefore, a stability analysis of the hydraulic falls ought to be performed.

Acknowledgement

This research was partially supported by EPSRC, the Leverhulme Trust, the National Science Foundation (NSF), Alliance (the Franco-British Joint Research Programme of the British Council, with Project Number 05697WF) and the European Commission's Improving Human Potential – Transnational Access to Research Infrastructures Programme. The second author wishes to thank the Centre National de la Recherche Scientifique (CNRS) for sponsoring his visit to École Normale Supérieure de Cachan in 2002.

Appendix. Conjugate states

In this appendix, we recall some global results on fronts (in the absence of an obstacle) and on conjugate flows (in the presence of an obstacle). The main purpose is to explain the origin of the special values of the Froude number $F = F_{\text{front}}$ and $F = F_{\max}$.

Fronts and conjugate flows are flows characterized by different uniform flows upstream and downstream. For simplicity, it is assumed that the upstream uniform flows have the same speed U in the upper and bottom layers. Given U, h_1^* and h_2^* upstream, one would like to know what are the possibilities for the uniform speeds and the layer thicknesses downstream (four unknowns). The conservation of mass fluxes in each layer provides two equations. The conservation of energy provides a third equation. The constraint that the channel height is constant provides a fourth equation. For fronts, the conservation of horizontal momentum flux provides a fifth equation.

Consequently, in the case of conjugate flows, one anticipates to be able to find nontrivial solutions for a continuous range of upstream Froude numbers and thickness ratios since there are four equations with four unknowns to be solved. For fronts, one

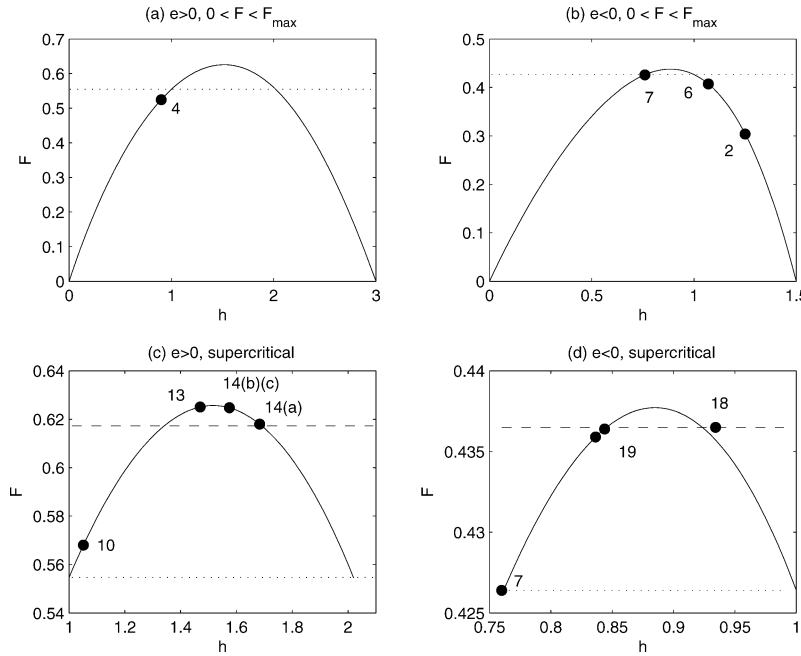

Fig. A.1. Plot of the Froude number F versus the ratio h between the downstream and the upstream bottom layer thicknesses. (a) Subcritical and supercritical flows with $\beta > \sqrt{\rho}$. The computations are performed with $\beta = 2$ and $\rho = 0.6$. For such parameter values, $F_{\text{bif}} = 0.555$, $F_{\text{front}} = 0.6173$ and $F_{\max} = 0.6256$. (b) Subcritical and supercritical flows with $\beta < \sqrt{\rho}$. The computations are performed with $\beta = 0.5$ and $\rho = 0.6$. For such parameter values, $F_{\text{bif}} = 0.4264$, $F_{\text{front}} = 0.4365$ and $F_{\max} = 0.4377$. There is always a maximum value $F_{\max}$ for the Froude number. (c) Same as (a), but restricted to supercritical flows. (d) Same as (b), but restricted to supercritical flows. The dotted lines represent the value of the Froude number F_{bif}, while the dashed lines represent the value of the Froude number F_{front}. The labels correspond to figure numbers. The label 18 is slightly off the curve because β was equal to 0.5046 instead of 0.5.

anticipates to find nontrivial solutions only for special upstream conditions. This is exactly what happens: fronts exist only if the upstream Froude number F is equal to $F = F_{\text{front}}$.

For conjugate flows, one finds the following relationship between the upstream Froude number F and the ratio $h = h_1^{\text{downstream}}/h_1^*$:

$$F^2 = \frac{2(1-\rho)}{(1+h)/h^2 + \rho(1+2\beta-h)/(1+\beta-h)^2}. \tag{A.1}$$

The relationship (A.1) can be easily obtained from Eqs. (A.3) and (A.8) in [27] together with the rigid lid constraint. Solutions to Eq. (A.1) are plotted in Fig. A.1. Clearly, there is a maximum Froude number $F_{\max}$ for conjugate flows.

References

[1] W.A.B. Evans, M.J. Ford, An integral equation approach to internal (2-layer) solitary waves, Phys. Fluids 8 (1996) 2032–2047.
[2] F. Dias, J.-M. Vanden-Broeck, Generalised critical free-surface flows, J. Engrg. Math. 42 (2002) 291–301.
[3] F. Dias, J.-M. Vanden-Broeck, Steady two-layer flows over an obstacle, Philos. Trans. Roy. Soc. London Ser. A 360 (2002) 2137–2154.
[4] D.M. Farmer, L. Armi, Maximal two-layer exchange over a sill and through the combination of a sill and contraction with barotropic flow, J. Fluid Mech. 164 (1986) 53–76.
[5] H. Sha, J.-M. Vanden-Broeck, Two-layer flows past a semicircular obstruction, Phys. Fluids A 5 (1993) 2661–2668.
[6] L.K. Forbes, Two-layer critical flow over a semi-circular obstruction, J. Engrg. Math. 23 (1989) 325–342.
[7] S.R. Belward, L.K. Forbes, Fully non-linear two-layer flow over arbitrary topography, J. Engrg. Math. 27 (1993) 419–432.
[8] F. Dias, J.-M. Vanden-Broeck, On internal fronts, J. Fluid Mech. 479 (2003) 145–154.
[9] J. Grue, H.A. Friis, E. Palm, P.-O. Rusås, A method for computing unsteady fully nonlinear interfacial waves, J. Fluid Mech. 351 (1997) 223–252.
[10] J.K. Sveen, Y. Guo, P.A. Davies, J. Grue, On the breaking of internal solitary waves at a ridge, J. Fluid Mech. 469 (2002) 161–188.
[11] P.-O. Rusås, J. Grue, Solitary waves and conjugate flows in a three-layer fluid, Eur. J. Mech. B Fluids 21 (2002) 185–206.
[12] S.S.-P. Shen, Forced solitary waves and hydraulic falls in two-layer flows, J. Fluid Mech. 234 (1992) 583–612.

[13] J.W. Choi, S.M. Sun, M.C. Shen, Steady capillary-gravity waves on the interface of a two-layer fluid over an obstruction-forced modified K–dV equation, J. Engrg. Math. 28 (1994) 193–210.
[14] J.W. Choi, S.M. Sun, M.C. Shen, Internal capillary-gravity waves of a two-layer fluid with free surface over an obstruction – forced extended KdV equation, Phys. Fluids 8 (1996) 397–404.
[15] R.H.J. Grimshaw, K.H. Chan, K.W. Chow, Transcritical flow of a stratified fluid: the forced extended Korteweg–de Vries model, Phys. Fluids 14 (2002) 755–774.
[16] H. Hanazaki, A numerical study of nonlinear waves in a transcritical flow of stratified fluid past an obstacle, Phys. Fluids A 4 (1992) 2230–2243.
[17] C.J. Knickerbocker, A.C. Newell, Internal solitary waves near a turning point, Phys. Lett. A 75 (1980) 326–330.
[18] E.R. Johnson, S.R. Clarke, Rossby wave hydraulics, Annu. Rev. Fluid Mech. 33 (2001) 207–230.
[19] S.R. Clarke, E.R. Johnson, The weakly nonlinear limit of forced Rossby waves in a stepped channel, Proc. Roy. Soc. London Ser. A 457 (2001) 2361–2378.
[20] S.R. Clarke, E.R. Johnson, Supercritical leaps in two-layer hydraulics, in: Proceedings 14th Australasian Fluid Mechanics Conference, Adelaide, Australia, 10–14 December 2001.
[21] P.G. Baines, Topographic Effects in Stratified Flows, Cambridge University Press, 1995.
[22] L.J. Pratt, On nonlinear flow with multiple obstructions, J. Atmospheric Sci. 41 (1984) 1214–1225.
[23] W.K. Melville, K.R. Helfrich, Transcritical two-layer flow over topography, J. Fluid Mech. 178 (1987) 31–52.
[24] O.A. Arntsen, Disturbances, lift and drag forces due to the translation of a horizontal circular cylinder in stratified water, Exp. Fluids 21 (1996) 387–400.
[25] O.A. Arntsen, Lee waves and hydrodynamical loads due to the motion of a submerged horizontal circular cylinder in a three-layer fluid, J. Hydraulic Res. 35 (1997) 435–453.
[26] G.A. Lawrence, The hydraulics of steady two-layer flow over a fixed obstacle, J. Fluid Mech. 254 (1993) 605–633.
[27] O. Laget, F. Dias, Numerical computation of capillary–gravity interfacial solitary waves, J. Fluid Mech. 349 (1997) 221–251.